ARTICLE

JOURNAL OF **Applied Polymer** WILEY
SCIENCE

Direct bonding and de-bonding on demand of polystyrene and polyamide surfaces, treated with oxygen plasma

Roman Günther[1,2] ⓘ | Walter R. Caseri[2] ⓘ | Christof Brändli[1] ⓘ

[1]Laboratory of Adhesives and Polymer
Materials, Institute of Materials and
Process Engineering, Zurich University of
Applied Sciences, Winterthur, Switzerland

[2]Laboratory for Multifunctional Materials,
Department of Materials, ETH Zurich,
Zurich, Switzerland

Correspondence

Christof Brändli, Laboratory of Adhesives
and Polymer Materials, Institute of
Materials and Process Engineering, Zurich
University of Applied Sciences, 8401
Winterthur, Switzerland.
Email: christof.braendli@zhaw.ch

Abstract

Smooth polystyrene (PS) and polyamide 12 (PA 12) surfaces were produced via an injection molding process followed by a smoothing process and subsequently treated with O_2 plasma to increase the number of polar groups capable of hydrogen bond formation on the surface. The presence of related groups was evident from X-ray photoelectron spectroscopy (XPS) and contact angle measurements. The sample topographies were investigated by atomic force microscopy (AFM). The plasma treatment allowed the joining of the substrates without adhesive by pressing the substrates together below or around the glass transition temperature. Notably, not only substrates of the same polymer but also PS and PA 12, which are incompatible, were joined with this method. The adhesion between the substrates was determined using a LUMifrac apparatus. The adhesion strength increased with increasing bonding temperature and when both substrates were plasma-treated, reaching adhesive strengths up to 5.5 ± 1.7 MPa. Remarkably, the joint substrates could be rapidly de-bonded on demand simply by treatment with water, and the separated substrates could be re-bonded by renewed plasma treatment.

KEYWORDS

adhesives, bonding, de-bonding, functionalization of polymers, surfaces and interfaces, thermoplastics

1 | INTRODUCTION

In the manufacture of microfluidic devices, adhesives are often avoided because adhesive residues can clog the channels.[1,2] One way to simplify this problem is to bond polymers together without adhesives.

Joining polymers by fusion bonding or welding is an established technology. By heating a polymer surface above its melting temperature (T_m), the molecules in the vicinity of the surface become mobile. When related polymer substrates are pressed together, the weld strength develops by a combination of surface rearrangement and interdiffusion of polymer chains.[3] However, the heat and pressure introduced to the polymer can damage the substrates if not controlled correctly.

To avoid these shortcomings, it is also possible to bond polymers together below their corresponding T_m or T_g. Partial interdiffusion of the polymer chains between surfaces,[4] which are in close contact or the action of intermolecular forces like van der Waals forces, dipole interactions, or

hydrogen bonds,[5] can lead to adhesive forces that are theoretically even stronger than what can be achieved with adhesives.[6] Interdiffusion of polymers around[7] or below T_g is possible for materials such as poly(methyl methacrylate),[8] PS,[9–12] or poly(phenylene oxide),[7,13] leading to adhesion between the respective substrates. However, the adhesive strength reached in these systems was relatively low, and the bonds were established in periods up to days. Such long bonding times render this technique less attractive for applications.

Surface treatments can reduce the bonding time and enhance the bonding strength by increasing the density of functional groups on the polymer surface. The most common treatment methods include UV irradiation,[14,15] corona discharge,[16–18] and plasma treatment.[15,19–26] The advantage of plasmas generated at low pressures is the large plasma volume established, allowing the modification of big objects with complex geometry. Moreover, the plasma is generated in a closed environment. Therefore, the gas can be chosen to match the desired functionalization.[27]

A precondition for direct bonding without adhesive is the presence of smooth substrate surfaces, as the interdiffusion of polymer chains and intermolecular forces can only act at short distances. A high roughness leads to repulsion between the substrates, and intermolecular interaction between the surfaces would only be possible at some contact spots.[28] An aspect that has hardly been investigated, except in some studies,[8,29–32] is the bonding of incompatible polymer interfaces with this technique. Bonding of incompatible polymers allows the stacking of layers from different materials to create more complex microfluidic devices. Despite new findings in adhesion,[4,20,33–39] it is still complicated to bond different types of polymers together. A direct bonding approach could provide a solution to related bonding challenges.

In this work, we address these issues on the example of PS and PA 12 and describe a novel reversible joining process without adhesive below T_g or T_m, respectively. PS is apolar, amorphous and transparent. Due to its facile microfabrication, PS is one of the most used thermoplastics for microfluidics and lab-on-a-chip applications.[39] PA 12 is polar and able to establish hydrogen bonds, partially crystalline and largely insoluble in common organic solvents. It is used as an incompatible model polymer to explore the possibilities of direct bonding of polar polymers and incompatible polymers pairings. Very smooth and flat substrate surfaces, as required for non-adhesive bonding, were produced by a novel combination of injection molding followed by a smoothing process. The obtained samples were then treated with O_2 plasma to increase the density of polar functional groups on the surfaces and the substrates were pressed together at different conditions without adhesive. The adhesive strength was determined by pull-out tests using a LUMifrac adhesion tester.[40] Moreover, separation of the bonded surfaces on-demand and reconnection of the separated surfaces was demonstrated, which is advantageous for cleaning or recycling the microfluidic devices after their use.

2 | EXPERIMENTAL

2.1 | Initial polymers purity and materials properties evaluation

PS (GP 585 X) was purchased from Synthos Chemical Innovations, Poland, and PA 12 (Grilamid L 16 nat) from EMS-Chemie, Switzerland. Since the polymers used are industrial products, the samples were investigated concerning purity and materials properties by NMR, inductively coupled plasma atomic emission spectroscopy (ICP-OES), gel permeation chromatography (GPC), differential scanning calorimetry (DSC), and dynamic mechanical thermoanalysis (DMTA). The methodology of these techniques can be found in the supporting information.

^{1}H NMR spectra did not show any unexpected signal (Figure S1). Therefore, significant amounts of additives in the polymers can essentially be excluded. Further, ICP-OES analysis did not show significant amounts of inorganic elements (Table S1). Thus, fillers or catalyst residues that could interfere with the tests seemed not to be relevant. Apparently, the polymers were present in pure form. GPC measurements showed a molecular weight of M_n 56,079 Da, M_w 218,167 Da, and M_n 30,560 Da, M_w 47,110 Da for PS and PA, respectively. DSC measurements disclosed a T_m of PA 12 of 184°C with a melting energy of -60 J g^{-1} (Figure S2). For PS, the T_g arose at 102°C. DMTA showed a T_g (maximum of tan delta) of PA 12 at 59°C (Figure S3). The storage and loss modulus of both polymers at different temperatures are summarized in Table 1. The storage modulus decreased with increasing temperature for both polymers, and therefore the material became softer at elevated temperatures.

2.2 | AFM

Atomic force microscopy (AFM) was performed with an NTEGRA AFM from NT-MDT Spectrum Instruments (Russia) in semi-contact mode (tapping mode) and Nova Px 3.5.0 software. NGS01 tips from NT-MDT Spectrum Instruments with a typical tip radius of 6 nm were used. The scan parameters were optimized using the ScanT software extension in the attractive measurement regime. Several scans over an area of 1×1, 10×10, and 100×100 μm^2 and a resolution of 512×512 pixels were performed for each sample. Each measurement line was

TABLE 1 Storage and loss modulus of PS and PA 12 at different temperatures measured with DMTA

Material	Temperature (°C)	Storage modulus (MPa)	Loss modulus (MPa)
PS	30	2703	51
	60	2465	65
	90	888	512
PA 12	30	1395	50
	60	458	65
	90	264	32
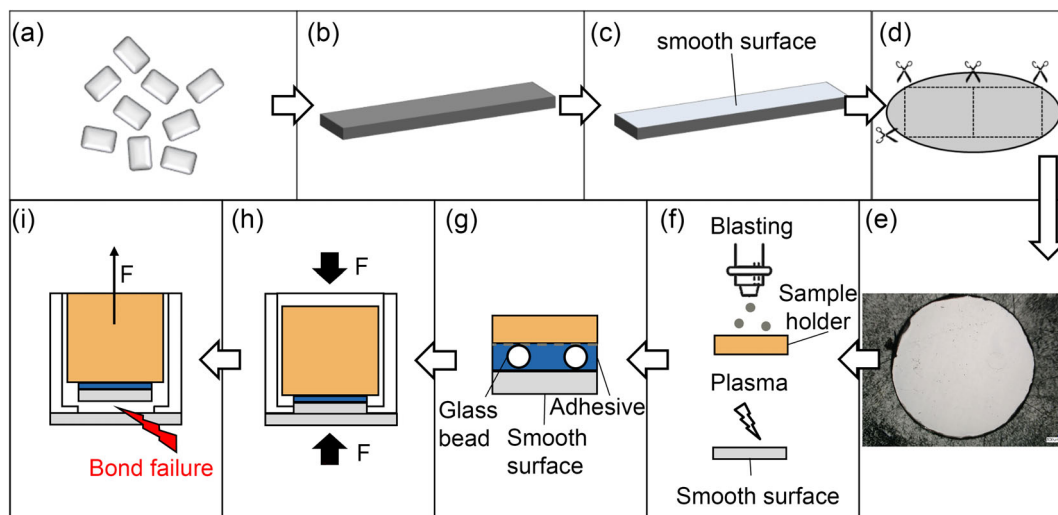
FIGURE 1 Sample preparation and assembly of specimens for LUMifrac testing. (a) Polymer granules are injection molded into (b) preforms. (c) Preforms after smoothing process are (d) cut or punched into (e) final form (PA sample). (f) The sample holder is sandblasted and cleaned with acetone. Plasma treatment of sample holder and backside of the sample. (g) Bonding of sample and sampleholder with adhesives. (h) Direct bonding of polymers by pressing two samples together. (i) Testing of adhesion with LUMifrac [Color figure can be viewed at wileyonlinelibrary.com]

recorded in two measuring directions. Based on the two images, a minimum was calculated, allowing to minimize the parachuting effect. Subsequently, the images were aligned using a first-order (1×1, 10×10 μm^2) or second-order (100×100 μm^2) line fit. The surface roughness was calculated using the integrated roughness analysis over the whole surface of the 10 x 10 μm^2 scans. The power spectral density (PSD) was calculated using fast Fourier transform analysis, following the procedure described in the work of Pastewka et al.[41] For a better visibility, the shown images were edited by peak cut-off.

2.3 | Surface treatment

Samples were treated in a Diener nano plasma furnace (Diener electronic GmbH + Co. KG, Germany) in oxygen for 12 s at 0.2 mbar pressure and 200 W power. The plasma furnace was run empty for 2 min before each treatment for cleaning and minimizing contamination.

2.4 | Fabrication of polymer substrates

In a first step, preforms (Figure 1b) with dimensions of $80 \times 10 \times 4$ mm^3 were prepared from the polymer granules (Figure 1a) in an injection molding process using a BOY XS injection molding machine from Dr. Boy GmbH & Co. KG, Germany. PS was injected at 240°C with 80 bar and PA at 250°C with 60 bar. The specimens were then smoothed by pressing them in a hot press (APV 2525, Herbert Meyer GmbH, Germany) against a silicon wafer (Dummy CZ-Si Wafer, MicroChemicals GmbH, Germany) for 30 s at 180°C (PS) or 185°C (PA) and 0.7 bar air pressure (corresponds to 1250 N). The hot samples were quenched with liquid nitrogen to prevent sticking to the wafer. The resulting 1.2 mm thick samples (Figure 1c) were cut to sizes with a circular saw in the case of PS (Figure 1d) or punched out to the desired size with a punching iron in the case of PA 12 (Figure 1e).

2.5 | Adhesion tests

Butt tensile tests (LUMifrac) were carried out with a centrifugal adhesion test analyzer from LUM GmbH (Germany) at room temperature. The assembly of the specimen is shown in Figure 1f-i. The aluminum sample holder (sandblasted and cleaned with acetone) and the backside of the small polymer sample (PS, 7×7 mm^2/PA 12, 8 mm diameter) were pre-treated with oxygen plasma for 30 s (Figure 1f) to insure high bond strength with two-component epoxy adhesive (Betamate 2090, DuPont, Switzerland). After treatment, the polymer samples were bonded with the adhesive to a 10 mm diameter sample holder. The thickness of the adhesive was adjusted to 0.2 mm with the aid of glass spheres (Figure 1g). After curing the adhesives for at least 24 h at room temperature, according to the manufacturer's suggestion, the sample holder was screwed in the copper weight and treated with oxygen plasma. After the plasma treatment, an aluminum sleeve was placed over the weight. The two polymer substrates were then pressed together in a hot press (Figure 1h) at temperatures from 30 to 90°C for periods between 30 and 900 s at 0.7 bar air pressure (corresponds to 1250 N). After pressing, the joint area (A) between all the specimens was manually measured with a digital measuring microscope and the internal software (VHX-6000 V3.0.0.116, Keyence). Because PS is transparent, the joint area was easily identified by a darker coloration (see Figure 5a, blue arrow). The samples were kept at room temperature in a dry atmosphere until tested in the LUMifrac device. For testing, six samples were loaded simultaneously in the measuring chamber. Through rotation, the applied centrifugal force yields a nearly pure butt tensile load to the specimen. The increase in load was set to 1 N s^{-1}. At bonding failure, the copper weight triggered the sensor, and the rotation speed of the centrifuge with the corresponding force at failure was recorded (Figure 1i). From the adhesive forces (F) and the joint areas (A), the adhesive strength (σ) of the joint was calculated (see Equation 1).

$$\frac{F}{A} = \sigma \qquad (1)$$

2.6 | Contact angle measurements

The advancing contact angles were measured using a DSA100 system and Advance Drop Shape (V1.8.0) Software by Krüss GmbH (Germany). Water, dimethyl sulfoxide (DMSO), and ethylene glycol droplets with a volume of 2 μl were placed onto the samples. At least seven droplets per liquid were deposited. The contact angles of the sessile drops were measured using an elliptical fit for contact angles greater than 20°. The height and width were measured manually for angles below, and the internal software calculated the contact angle. To determine the surface free energy (SFE), the Owens-Wendt-Rabel-Kaelble method (OWRK)[42,43] was applied with the internal software.

2.7 | XPS

X-ray photoelectron spectroscopy (XPS) was performed with a SPECS™ spectrometer (SPECS GmbH, Germany) using a Mg Kα X-ray source ($\lambda = 1253.6$ eV) with a power of 300 W. The measurements were made at room temperature. Each sample was studied at one spot. The investigated area amounted typically to 7×10 mm^2. Survey spectra were acquired over a binding energy range of 0–1000 eV at a pass energy of 30 eV and resolution of 0.5 eV/step. High-resolution spectra of C 1 s were obtained as an average of three scans acquired at pass energy of 20 eV and resolution of 0.05 eV/step. The CasaXPS software was used for background subtraction (U 2 Tougaard-type), peak integration, quantitative chemical analysis, and deconvolution. The adventitious C 1 s peak at 285 eV was used to calibrate the binding energy scale.

3 | RESULTS AND DISCUSSION

3.1 | Topography

The topography of the polymer surfaces was investigated using AFM. The 3-D information obtained can be used to determine the roughness over different orders of magnitude. Thus, it is also possible to investigate the influence of the plasma treatment (see Figure 2). No changes were visible by eye for PS before and after plasma treatment, and the RMS surface roughness (S_q) did not change significantly upon plasma treatment (2.7 and 3.3 nm, respectively). PA 12 showed a similar morphology. Again, no changes in topography were visible after plasma treatment and S_q remained essentially unchanged (3.4 and 3.5 nm, respectively, before and after plasma treatment).

A more detailed view of the roughness is possible in the PSD plot. The PSD of a surface is a mathematical method that divides a surface into contributions from different spatial frequencies (wave vectors). Here, the PSD is a Fourier transform of the autocorrelation function of the measured signal, which contains only the power (without the phase) over a range of wave vectors. This allows the identification of spatial frequencies in the signal. The
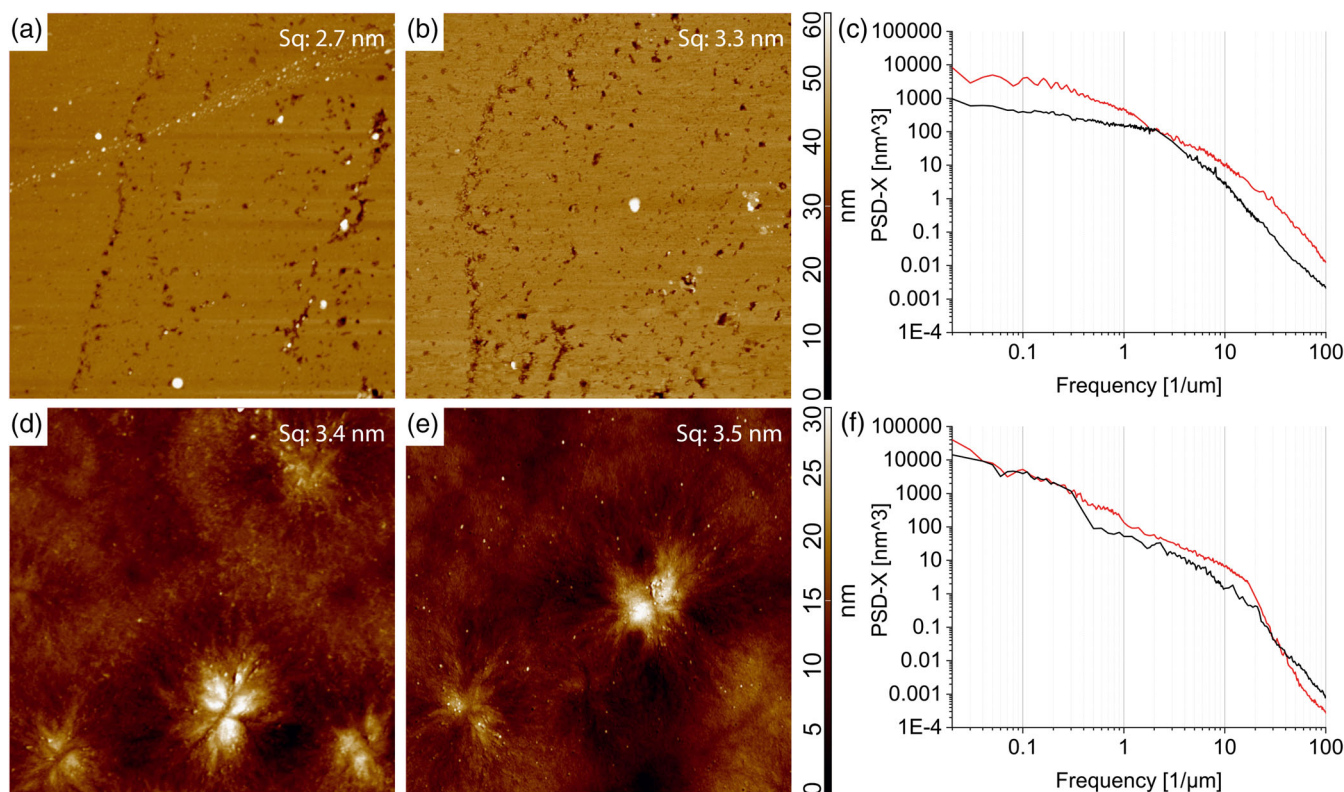
FIGURE 2 AFM images and PSD of PS and PA 12 before and after oxygen plasma treatment. The edge length of all AFM images is 10 μm. (a) PS surface after hot pressing against a silicon wafer, before plasma activation, surface roughness $S_q = 2.7$ nm. (b) PS surface after plasma activation $S_q = 3.3$ nm. (c) PSD of PS surfaces before (black), after plasma treatment (red). (d) PA 12 surface after hot pressing against a silicon wafer before plasma activation, $S_q = 3.4$ nm. (e) PA 12 surface after plasma activation, Sq = 3.5 nm. (f) PSD of the PA 12 surfaces before (black), after plasma treatment (red) [Color figure can be viewed at wileyonlinelibrary.com]

advantage of PSD is that the statistical information of the surface topography is mainly unaffected by the choice of a particular scan size and pixel resolution.[41]

In Figure 2c + f, the roughness was determined over several orders of magnitude by AFM measurements and summarized in a PSD. The roughness of the PS increased slightly over all orders of magnitude during plasma treatment (higher signal in the PSD). For PA 12, the roughness did not increase significantly over the whole spectrum.

3.2 | Surface chemistry

Advancing contact angle measurements (see Figure 3) showed a value of $90 \pm 2°$ (95% confidence interval) for water on PS. After plasma treatment, this value decreased to $11 \pm 4°$. The SFE increased from 35 ± 3 to 71 ± 9 mN m^{-1}. The same effect was observed with PA 12. Here, the contact angle decreased from $60 \pm 2°$ to $49 \pm 2°$, and the SFE increased from 29 ± 4 to 48 ± 7 mN m^{-1}. Thus, both surfaces became more polar upon surface treatment, but the effect is less pronounced for PA 12 than for PS since

PA already contained polar groups before plasma treatment.

The cause of the changes in contact angles and surface energies can be investigated in more detail with XPS (see Figure 4). The XPS studies showed that plasma treatment led to an increase in oxygen concentration and functional groups on the surfaces of both polymers. In fact, an increase from 1% to 21% oxygen was observed for PS and from 7% to 19% for PA 12. A more detailed examination of the C 1 s signal provides more information. Thus, in PS, additional signals from hydroxyl (14% of C atoms), carbonyl (2% of C atoms), and carboxyl (8% of C atoms) groups were detected. In PA 12, an increase in polar groups on the surface was also evident. As expected, polar groups were already detected in PA 12 before plasma treatment, but additional hydroxyl groups (related to 8% of the C atoms) were generated on the surface. In comparison, the content of carboxyl groups did not change significantly (an increase of 1% related to the C atoms). The signals of carbonyl and overlapping amide groups increased from 8% of C atoms to 14% of C atoms assuming that the increase is mainly based on carbonyl groups.
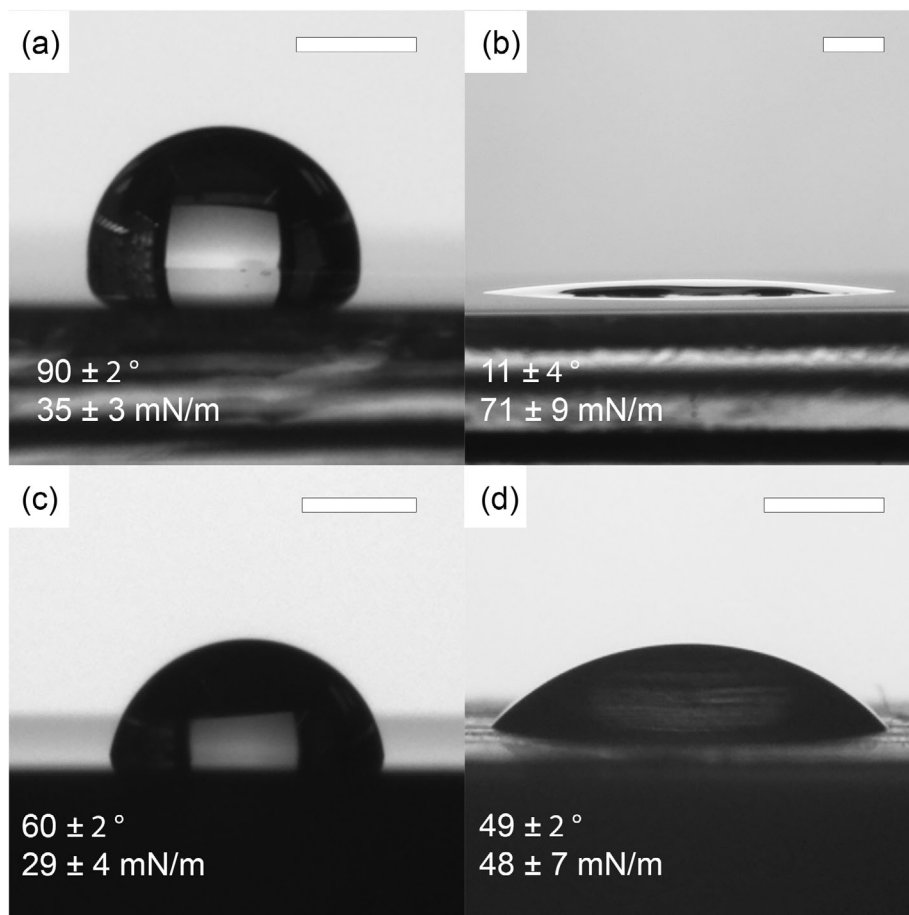
FIGURE 3 Advancing contact angle measurements of water on polymer substrates. The contact angles and SFE are indicated at the left lower corner in each image. The scale bar represents 1 mm (a) water on PS without plasma activation. (b) Water on PS after plasma treatment. (c) Water on PA 12 without plasma activation. (d) Water on PA 12 after plasma treatment

Despite a similar oxygen concentration on the surface, PS shows a higher wettability after plasma treatment compared to the equally treated PA. The difference in the wettability can be explained by the functional groups created during the plasma treatment. For PS, more hydroxyl- and carboxyl groups were introduced than for PA. Accordingly, hydroxyl- and carboxyl groups affect the SFE and the contact angle stronger than carbonyl groups.

The topography and surface chemistry measurements showed that plasma treatment is a suitable method to introduce functional groups to the surface without increasing the roughness of the polymer significantly.

3.3 | Bonding and de-bonding

In the first series of tests, a PA 12 surface was bonded to a PS surface. For this purpose, both surfaces were treated with oxygen plasma. Adhesion between the surfaces was achieved in all cases (30 to 90°C and 30 to 900 s). The results (see Table 2) showed that the joint area and the adhesive force increased with increasing temperature. However, the adhesive strength decreased. It is also noticeable that the results at 30°C showed a large variance, decreasing with increasing temperature. Variations of the bonding time showed no significant changes in the results. Therefore, it can be assumed that the bonding process was faster than 30 s.

Figure 5d-i shows the fractured surfaces after the LUMifrac test. The specimens failed at 30 and 60°C in the joint plane. At 30°C, no material was transferred from one substrate to the other. At 60°C, however, material was transferred, with small pieces of PS sticking to the PA 12. This is obvious from the dark areas on the images (Figure 5e + h indicated by red arrows and Figure 6b). At 90°C, however, a failure of the PS occurred. At this temperature, the bond did not fail in the joint plane, as at the lower temperatures, but within the material. The crack propagated in the bulk material leading to a cohesive failure. Here, material was transferred from one sample to the other. Therefore, it can be concluded that the adhesive forces between the surfaces were more pronounced than within the material itself. This also explains the lower adhesive strengths since the material itself failed before the joint.

When the PS fracture surface of the sample bonded at 30°C (Figure 5g) was examined more closely, the imprint
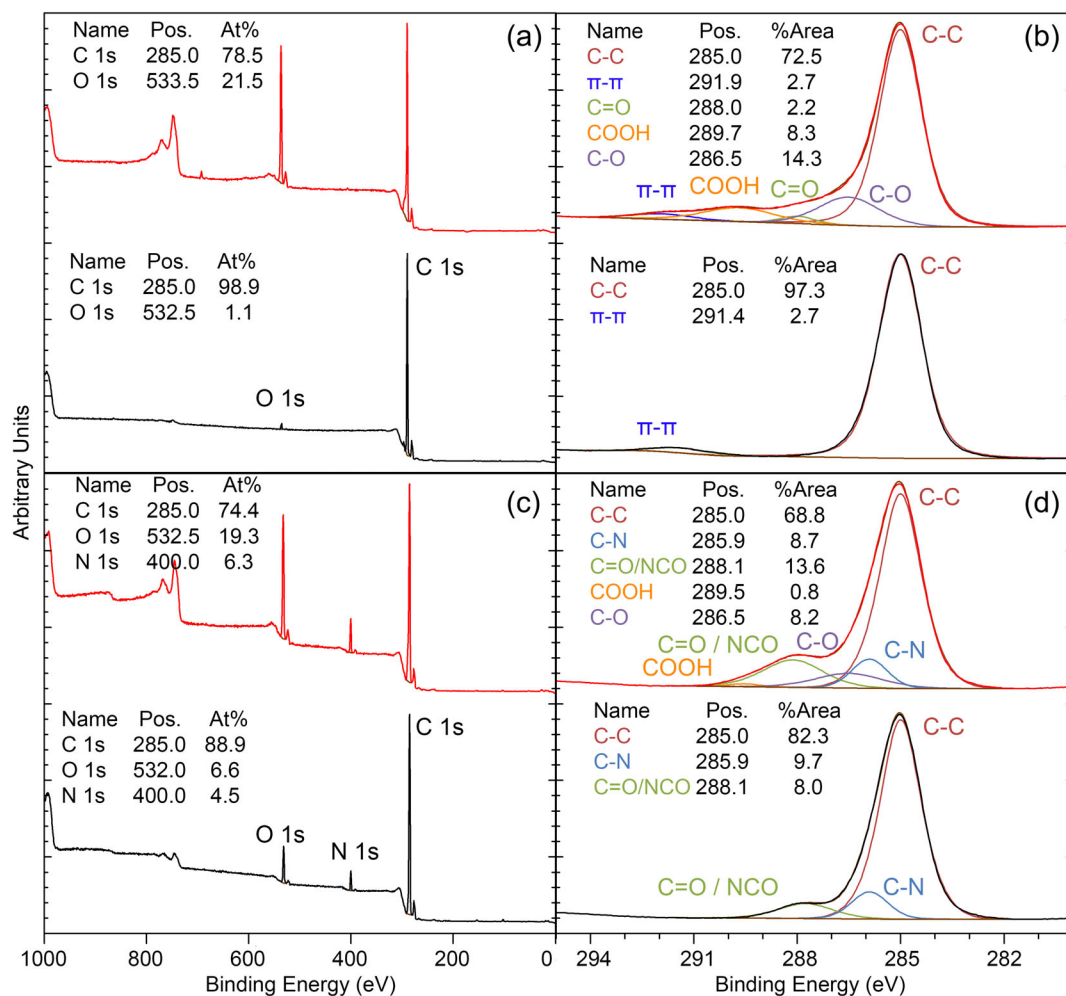
FIGURE 4 XPS data before (black curve) and after plasma treatment (red curve) of PS and PA 12. (a) and (b) PS, (c) and (d) PA 12 [Color figure can be viewed at wileyonlinelibrary.com]

of the PA 12 plate was visible. A dark outer area appeared, which became lighter towards the center until a dark spot (indicated by a blue arrow) emerged in the center. The dark spot in the center corresponds to the joint area shown in Figure 5a. The outer area was formed during unloading the press after the bonding process and could only be observed on plasma-treated surfaces. It must be assumed that the specimens were very smooth but had a slight curvature on a larger length scale. During bonding, the specimens were pressed against each other with high force. The specimen surfaces were elastically deformed, and both specimen surfaces encountered over the entire surface and were bonded to each other. When the specimens were unloaded after the bonding process, the surfaces relaxed, and the bond between the surfaces broke. Accordingly, a joint area remained. These observations are consistent with the findings of Johnson, Kendall, and Roberts (JKR) and their contact mechanics model.[44,45] On closer inspection, the outer area of the fracture had a rippled pattern reminiscent of the

structure of a record (see Figure 6a). This is due to a stick–slip fracture mechanism described in detail in the literature.[14]

This effect also explains the increased joint area and adhesion forces with increasing pressing temperature. When the temperature increased, the materials softened (see Table 1 and Figure S3). Due to the lower storage modulus, the materials can deform plastically and thus compensate for the unevenness in the surfaces. The higher joint area also induces greater adhesive forces between the surfaces. This also explains the large variance in the results at 30°C. Here, the joint areas and adhesive forces achieved were small, that interfering factors such as handling the specimens and the friction of the copper weight in the cylinder during the measurement strongly influenced the results. Some samples broke during handling and while inserting in the LUMifrac. The friction of the copper weight in the aluminum sleeve reached values up to 0.5 N.
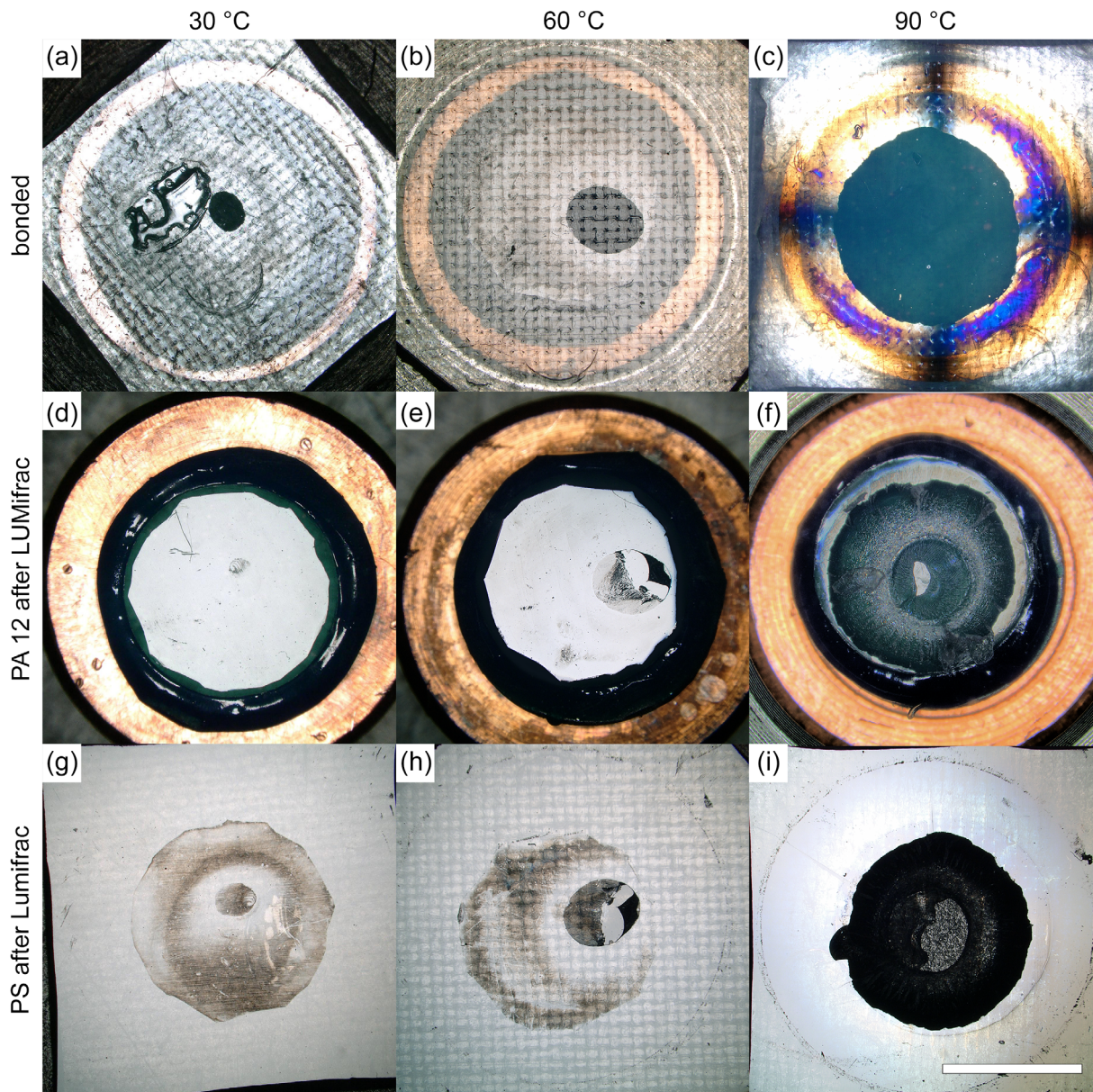
FIGURE 5 Contact points and fracture patterns of connected specimens and after testing with the LUMifrac device. The white scale bar corresponds to 5 mm. First column (a, d, g) bonded at 30°C, second column (b, e, h) bonded at 60°C, third column (c, f, i) bonded at 90°C. (a-c) Joint area of the bonded PS and PA 12. (d-f) PA 12 surface after LUMifrac testing. (g-h) PS after LUMifrac testing. The blue arrow indicates the remaining contact spot after bonding. The red arrow indicates material transfer of PS to PA [Color figure can be viewed at wileyonlinelibrary.com]

TABLE 2 Joint area, adhesive force, and adhesive strength of the joint as a function of the pressing parameters, for PA-PS material combination (variance: *t* student, 95% confidence interval, $n = 6$)

Bondingtemp. (°C)	Bondingtime (s)	Jointarea (mm²)	Adhesive force (N)	Adhesive strength (MPa)
30	30	1.4 ± 1.2	5.6 ± 1.6	4.6 ± 4.7
	900	1.9 ± 0.7	7.6 ± 5.0	4.5 ± 3.8
60	465	16.4 ± 6.4	59.4 ± 8.7	4.0 ± 1.1
90	30	41.3 ± 3.7	84.3 ± 4.6	2.1 ± 0.2
	900	38.2 ± 1.5	72.1 ± 5.6	1.9 ± 0.2

FIGURE 6 AFM images of PA 12 after LUMifrac testing. The edge length of all AFM images is 100 μm. (a) Outer area of the fracture pattern. Rippled pattern reminiscent of the structure of a record. (b) Big pieces of PS still stick to the surface of PA 12 [Color figure can be viewed at wileyonlinelibrary.com]
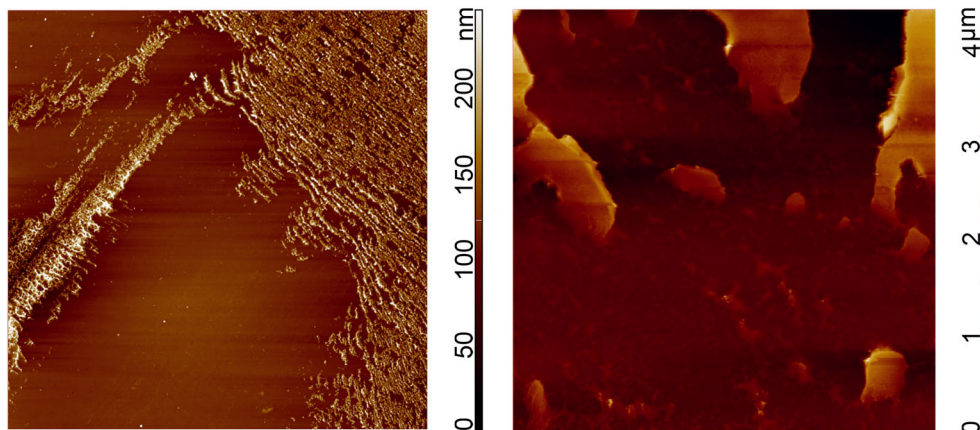
TABLE 3 Joint area, adhesive force, and adhesive strength of the joint with bonding time of 30 s and bonding temperature of 60°C as a function of the bonding setup. (variance: t student, 95% confident interval, $n = 6$)

Materials	Plasma treated	Joint area (mm^2)	Adhesive force (N)	Adhesive strength (MPa)
PS-PS	Both	25.7 ± 7.4	42 ± 12.7	1.6 ± 0.2
	One side	n. a.	n. a.	n. a.
	None	n. a.	n. a.	n. a.
PA-PA	Both	31.2 ± 3.7	37.1 ± 7.3	1.2 ± 0.2
	One side	7.7 ± 2.2	2.8 ± 1.2	0.4 ± 0.2
	None	n. a.	n. a.	n. a.
PA-PS	Both	9.3 ± 4.6	46.4 ± 14.4	5.5 ± 1.7
	PS	3.3 ± 0.1	2.6 ± 0.4	0.8 ± 0.1
	PA	n. a.	n. a.	n. a.
	None	n. a.	n. a.	n. a.

Abbreviation: n.a., no adhesion.

For further tests, the bonding parameters 30 s at 60°C were therefore selected. Since the specimens failed at this temperature within the joint plane and the results showed a smaller variance than at 30°C.

The second series of tests examined the influence of plasma activation and material combination on the bond. For this purpose, 2 PS surfaces (PS-PS), 2 PA 12 surfaces (PA-PA), and 1 PS with 1 PA 12 surface (PA-PS) were directly bonded. Furthermore, for the equal substrate PS-PS and PA-PA pairings, none, one, or both surfaces were treated with oxygen plasma. For the PS-PA pairings, none, PA 12, PS, or both surfaces were treated with plasma. The joint area, adhesive force, and adhesive strength as a function of the bonding parameters are summarized in Table 3.

If no surface was treated with plasma, no adhesion between the substrates could be detected in all cases. Also, no adhesion between the PS-PS substrates could be achieved when only one side was plasma-treated with oxygen plasma. However, a large joint area and high adhesive strength between substrates could be obtained when both sides were treated. For PA-PA systems, a small joint area and low adhesive strength were observed when only one side was treated. When both sides were treated with plasma, a large joint area and high adhesive strength between the substrates could also be obtained. For the PA-PS material pairing, no bonding could be obtained when only PA 12 was plasma-treated. When only PS was plasma-treated, a small joint area and low adhesive strength were obtained. A joint area smaller than the corresponding equal polymer pairings resulted when both PA 12 and PS were plasma-treated, but despite this, the highest adhesive forces and the highest adhesive strengths were attained.

3.3.1 | De-bonding on demand

De-bonding of joint polymers was attempted by treatment with solvents in which both PS and PA 12 are insoluble. A polar solvent (water, Video S1) and a non-polar solvent (hexane, Video S2) were dropped onto the joint plane of

PS and PA 12 substrates. The solvents immediately penetrated into the bond plane, probably promoted by capillary forces. When water was dropped onto the joint face, the bond detached within seconds, the dead weight of the specimen holder and the copper weight (equivalent to about 0.16 N) were sufficient to separate the surfaces. This corresponded to the weakening of the bond strength by more than 99%. However, when hexane was dropped on the joint face, no decay of the joint system was observed after 30 min. When the samples were then forcefully separated by hand the PS failed cohesively and material was transfers from one substrate to the other.

The results of the bonding and de-bonding experiments indicated that the interdiffusion of the polymer chains during the pressing process should be excluded as the main reason for adhesion. Although Boiko et al.[7] showed that bonding samples through interdiffusion below T_g or T_m is possible, these processes are time-dependent and commonly slower than the bonding times applied in the experiments performed here. Furthermore,

as the bonding proceeded with incompatible polymers also speaks against interdiffusion as the primary bonding mechanism since the polymer chains are immiscible and do not interpenetrate each other.

Likely, hydrogen bonds contribute considerably to the adhesion of the plasma-treated polymers. Hydrogen bonds form quickly and can therefore establish during the time applied period for joining the polymers. Significant adhesion was only observed for the PS-PS systems when both substrates had been treated with oxygen plasma. This is again in line with an essential role of hydrogen bonds since hydrogen bonds can only develop when both substrates contain functional groups that are amenable to this type of bond.

For PA 12, polar groups are present on the surface even without plasma treatment, yet 2 PA 12 surfaces could not be bonded if neither side had been plasma-treated. However, when one side was treated with oxygen plasma, considerable adhesion between substrates was found. The number of sites capable of establishing
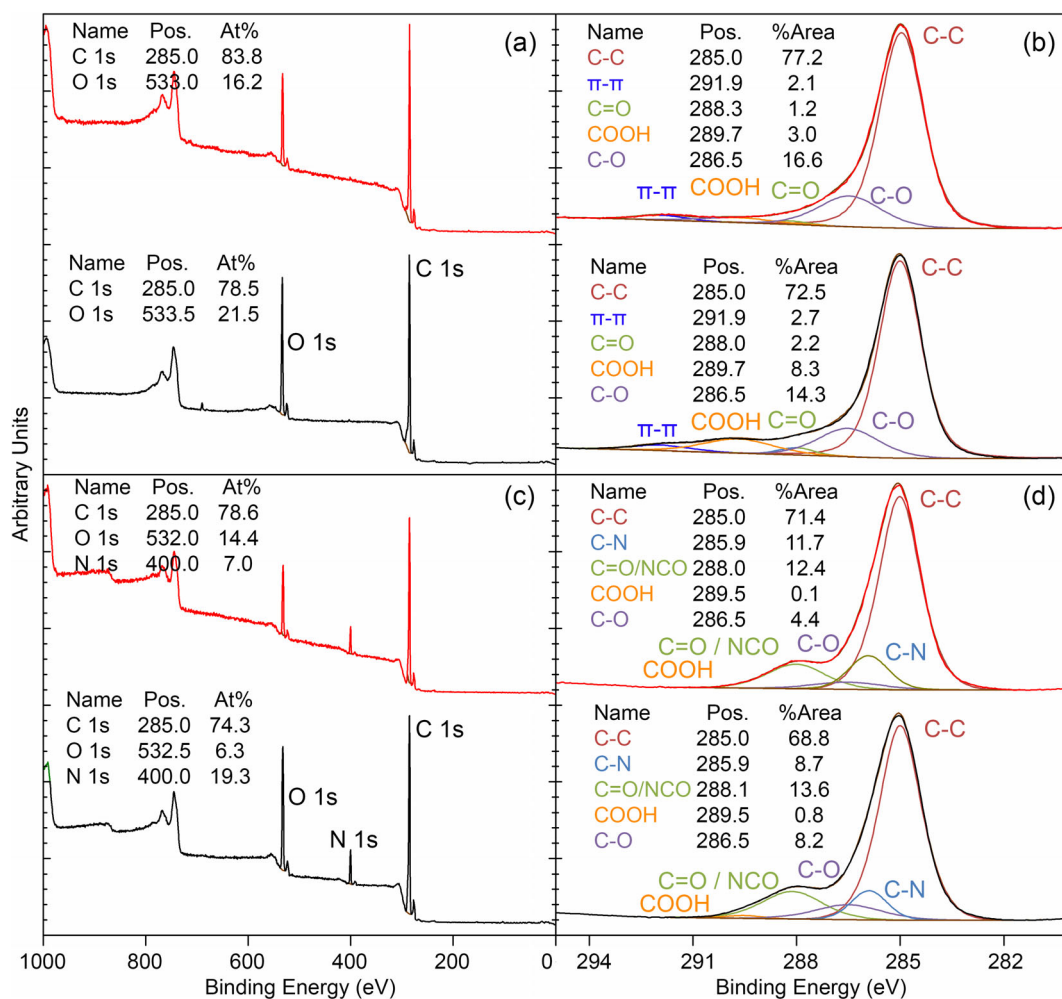

FIGURE 7 XPS data of polymer substrates after washing with water. Black curve: Directly after plasma treatment. Red curve: Plasma-treated, washed with water and dried. (a) Und (b) PS. (c) Und (d) PA 12 [Color figure can be viewed at wileyonlinelibrary.com]

TABLE 4 Joint area, adhesive force, and adhesive strength of the joint: Comparison between bonded and re-bonded surfaces. (variance: t student, 95% confident interval, $n = 6$)

| Materials	Bonding	Joint area (mm²)	Adhesive force (N)	Adhesive strength (MPa)
PA-PS	1st bonding	9.3 ± 4.6	46.4 ± 14.4	5.5 ± 1.7
	Re-bonding	3.2 ± 1.9	11.8 ± 11.1	3.6 ± 1.5
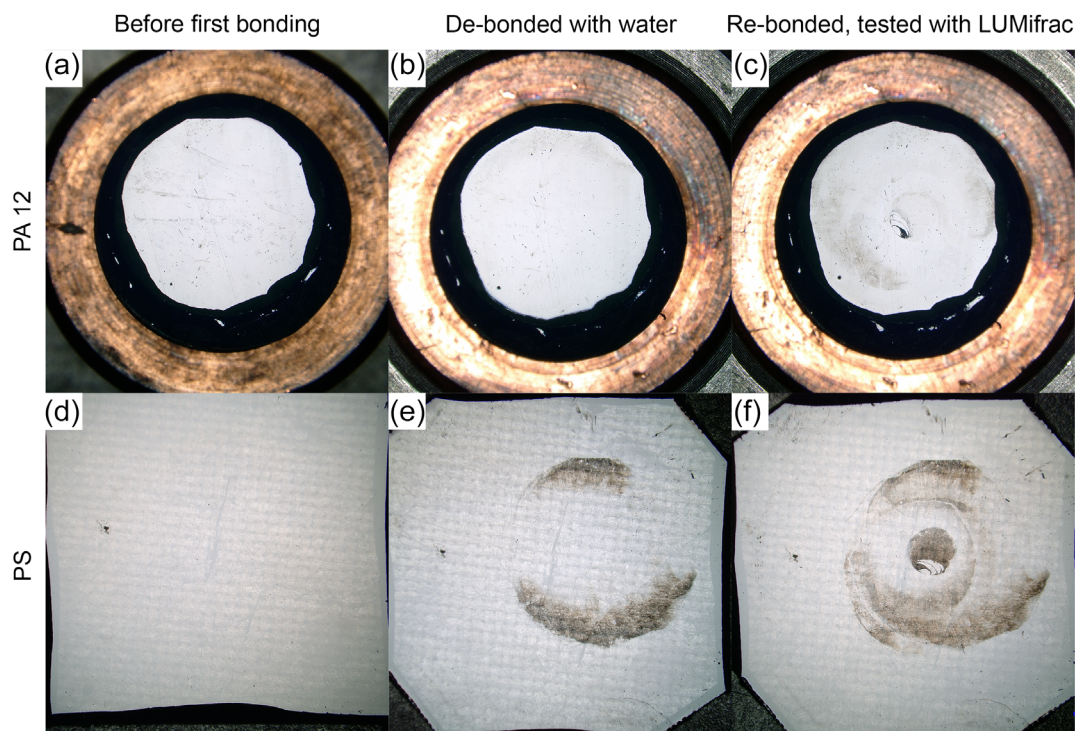
FIGURE 8 Polymer samples during the re-bonding procedure. (a+d) before the first bonding. (b+e) after de-bonding with water. (c+f) after re-bonding again and forced separation using a LUMifrac apparatus. The dark areas show material transfer between the surfaces. The white scale bar corresponds to 5 mm [Color figure can be viewed at wileyonlinelibrary.com]

hydrogen bonds between the surfaces was possibly too low without plasma treatment. Accordingly, when both surfaces were plasma-activated, the number of groups capable of establishing hydrogen bonds probably increased since the best adhesion was observed for the PA-PA systems in this case. The substrates could not be bonded for the PA-PS system if neither or only the PA 12 substrate had been plasma-treated. Here, no sites capable of hydrogen bonding were present on both or one side, respectively. When the PS substrate was treated, considerable adhesion between the substrates was achieved due to the presence of functional groups capable of hydrogen bonding on both substrates. When additional functionalities were introduced by plasma treatment on both substrates, the adhesive strength increased, reaching the highest adhesive strength measured for all systems.

The fact that de-bonding of the surfaces arose with water but not with hexane is also consistent with a dominant presence of hydrogen bonds. Water molecules can readily break hydrogen bonds, in contrast to hexane.[17]

De-bonded samples were dried and examined by XPS (Figure 7). Compared to freshly plasma-treated samples, the oxygen concentration on the surfaces decreased by 5% in each case, for PS from 21% to 16% and for PA 12 from 19% to 14%. The C 1 s signal in the case of PS revealed mainly a reduction of carboxyl groups from 8% to 3% of C atoms. For PA 12, the carbonyl or the overlapping amide groups were reduced from 14% to 12% of C atoms and the carboxyl groups from 1% to 0% of C atoms. Besides, the proportion of hydroxyl groups was also reduced from 8% to 4%. Therefore, the density of polar groups and groups which can form hydrogen bonds decreased. A wash-off of these groups can explain the reduction of oxygen and the corresponding functional groups. Chain scissoring can occur during plasma
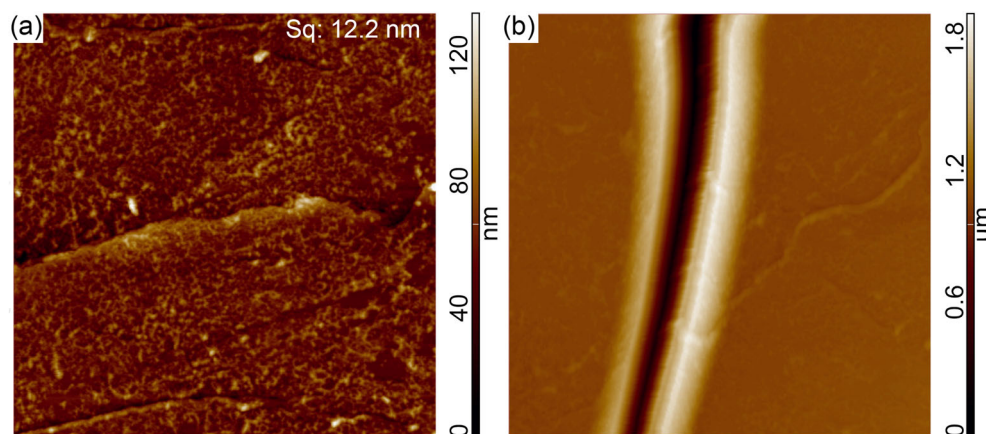
FIGURE 9 AFM images of PS after de-bonding with water. The edge length of all AFM images is 10 µm. (a) Darker areas with enhanced roughness similar to Figure 8e, surface roughness $S_q = 2.7$ nm (b) scratch found on the sample [Color figure can be viewed at wileyonlinelibrary.com]

treatment and reduce the molecular weight of the polymers, leading to smaller and functionalized polymer chains.[46] The polar groups increase the solubility of the chain fragments and are removed during the washing process.

3.3.2 | Re-bonding

Attempts were made to reconnect dried de-bonded samples directly in the same way as the plasma-treated samples, but this was not successful. This could be due to the decreased density of polar groups and groups capable of hydrogen bond formation upon de-bonding (see above). However, when the samples were treated again with oxygen plasma, the substrates could be reconnected.

The joint area, adhesive force, and adhesive strength after re-bonding the samples are summarized in Table 4 and compared with values of initially joint specimens. It turned out that all the values of re-bonded samples were reduced.

Further, the morphology of the specimens after de-bonding on-demand and re-bonding were examined with a microscope (see Figure 8). Upon de-bonding, the samples underwent a change in morphology in the edge region. However, little change was evident in the inner part of the joint area. The patterns in the edge area after de-bonding were also observed in Figure 5. After de-bonding, the surface became rougher with Sq = 12.2 nm (see Figure 9a), showed some scratches (Figure 9b) and thus made re-bonding more difficult. This resulted in a smaller joint area and correspondingly smaller adhesive force and adhesive strength.

When analyzing the fractured surface after re-bonding, it appeared that the failure mechanism did not change compared to the first bonding. Again, material was transferred from the PS side to the PA 12 substrate. This indicates that the re-bonding works well despite the increased roughness of the sample.

4 | CONCLUSIONS AND OUTLOOK

This work shows that plasma treatment of 12 s is introducing functional groups on the PS and PA 12 surfaces. During this treatment, the topography of the substrates is not changed significantly. The resulting functional groups on the polymer surfaces enable the samples to be firmly bonded together. Pressing at evaluated temperatures increases the contact area between the substrates and increases the adhesive force. It is possible to bond not only substrates of the same polymers but also incompatible polymers, on the example of PS and PA 12, reversibly and without adhesives. Likely, hydrogen bonds playing a considerable role in the binding mechanism. It is also evident that de-bonding on demand can be achieved within seconds by treatment with water and can afterward be re-bonded by renewed plasma treatment.

The bonding technique presented shows a possibility to manufacture PS-based and multi-material microfluidic devices for non-polar solvents. The de-bonding with water allows facile disassembly of the device for cleaning or recycling at the end of its lifetime. Further research is needed to develop methods to trigger a de-bonding with other solvents.

ORCID
Roman Günther https://orcid.org/0000-0003-4836-7269
Walter R. Caseri https://orcid.org/0000-0002-5165-5299
Christof Brändli https://orcid.org/0000-0002-1474-8453

REFERENCES
[1] R. Arayanarakool, S. Le Gac, A. Van Den Berg, *Lab Chip* **2010**, *10*, 2115.
[2] E. P. Dupont, R. Luisier, M. A. M. Gijs, *Microelectron. Eng.* **2010**, *87*, 1253.
[3] R. P. Wool, B. Yuan, O. McGarel, *J. Polym. Eng. Sci.* **1989**, *29*, 1340.

[4] F. Awaja, *Polymer* **2016**, *97*, 387.

[5] J. N. Israelachvili, *Intermolecular and Surface Forces*, Elsevier, **2011**.

[6] K. Kendall, *Molecular Adhesion and Its Applications*, Kluwer Academic Publishers, **2004**.

[7] Y. M. Boiko, R. E. Prud'homme, *J. Polym. Sci. Part B Polym. Phys.* **1998**, *36*, 567.

[8] Y. M. Boiko, J. Lyngaae-Jørgensen, *J. Macromol. Sci. Phys.* **2004**, *43*, 695.

[9] Y. M. Boiko, *Colloid Polym. Sci.* **2016**, *294*, 1237.

[10] Y. M. Boiko, R. E. Prud'homme, *J. Macromol. Sci. Phys.* **2005**, *44*, 413.

[11] Y. M. Boiko, A. Bach, J. Lyngaae-Jørgensen, *J. Polym. Sci. Part B Polym. Phys.* **2004**, *42*, 1861.

[12] Y. M. Boiko, *J. Adhes.* **2019**, *95*, 796.

[13] Y. M. Boiko, R. E. Prud'homme, *J. Appl. Polym. Sci.* **1999**, *74*, 825.

[14] H. Zeng, J. Huang, Y. Tian, L. Li, M. V. Tirrell, J. N. Israelachvili, *Macromolecules* **2016**, *49*, 5223.

[15] H. Shinohara, J. Mizuno, S. Shoji, *Sens. Actuators, A Phys.* **2011**, *165*, 124.

[16] C. Y. Kim, J. Evans, D. A. I. Goring, *J. Appl. Polym. Sci.* **1971**, *15*, 1365.

[17] D. K. Owens, *J. Appl. Polym. Sci.* **1975**, *19*, 265.

[18] D. K. Owens, *J. Appl. Polym. Sci.* **1975**, *19*, 3315.

[19] S. Zhang, F. Awaja, N. James, D. R. McKenzie, A. Ruys, *J. Polym. Adv. Technol.* **2011**, *22*, 2496.

[20] F. Awaja, T. Wong, B. Arhatari, *Biomed. Microdevices* **2018**, *20*, 7.

[21] S. Zhang, F. Awaja, N. James, D. R. McKenzie, A. Ruys, *J. Colloids Surf. A Physicochem. Eng. Aspects* **2011**, *374*, 88.

[22] K. S. Chen, U. Yoshikimi, I. Yoshito, *J. Adhes. Sci. Technol.* **1992**, *6*, 1023.

[23] S. Roy, C. Y. Yue, *Plasma Processes Polym.* **2011**, *8*, 432.

[24] J. Mizuno, S. Farrens, H. Ishida, V. Dragoi, H. Shinohara, T. Suzuki, M. Ishizuka, T. Glinsner, S. Shoji, *ICMENS* **2005**, *2005*, 346.

[25] N. V. Bhat, D. J. Upadhyay, *J. Appl. Polym. Sci.* **2002**, *86*, 925.

[26] R. Foerch, G. Kill, M. J. Walzak, *J. Adhes. Sci. Technol.* **1993**, *7*, 1077.

[27] J. Pinson, D. Thiry, *Surface modification of polymers: Methods and applications*, (Eds: J. Pinson, D. Thiry), Wiley-VCH Verlag GmbH & Co. KGaA, New Jersey **2019**.

[28] L. Pastewka, M. O. Robbins, *Proc. Natl. Acad. Sci. U. S. A.* **2014**, *111*, 3298.

[29] Y. M. Boiko, *Polym. Bull.* **2020**. https://doi.org/10.1007/s00289-020-03451-6

[30] Kogoma, M.; Manabe, A.; Tanaka, K. 19th International Symposium on Plasma Chemistry; **2009**.

[31] Y. Ohkubo, K. Endo, K. Yamamura, *Sci. Rep.* **2018**, *8*, 1.

[32] Y. M. Boiko, *Polym. Bull.* **2020**, *77*, 6377.

[33] J. Israelachvili, Y. Min, M. Akbulut, A. Alig, G. Carver, W. Greene, K. Kristiansen, E. Meyer, N. Pesika, K. Rosenberg, H. Zeng, *Rep. Prog. Phys.* **2010**, *73*, 036601.

[34] T. Utzig, S. Raman, M. Valtiner, *Langmuir* **2015**, *31*, 2722.

[35] J. M. Eagan, J. Xu, R. Di Girolamo, C. M. Thurber, C. W. Macosko, A. M. La Pointe, F. S. Bates, G. W. Coates, *Science* **2017**, *355*, 814.

[36] M. Gonda, T. Utsunomiya, T. Ichii, H. Sugimura, *Int. J. Adhes. Adhes.* **2020**, *100*, 102604.

[37] T. H. Yang, Y.-S. Chiu, C.-Y. Yang, A. Shigetou, C. R. Kao, *Trans. Japan Inst. Electron. Packag.* **2019**, *12*, E19.

[38] P. N. Immanuel, C. C. Chiang, C. R. Yang, M. Subramani, T. H. Lee, S. J. Huang, *J. Micromech. Microeng.* **2021**, *31*, 31.

[39] C. Wang, X. Qi, Y. Wang, B. Wu, Y. Tian, *J. Electrochem. Soc.* **2018**, *165*, B3091.

[40] U. Beck, G. Reiners, D. Lerche, U. Rietz, H. Niederwald, *Surf. Coat. Technol.* **2011**, *205*, S182.

[41] T. D. B. Jacobs, T. Junge, L. Pastewka, *Surf. Topogr. Metrol. Prop.* **2017**, *5*, 5.

[42] D. K. Owens, R. C. Wendt, *J. Appl. Polym. Sci.* **1969**, *13*, 1741.

[43] D. H. Kaelble, *J. Adhes.* **1970**, *2*, 66.

[44] K. L. Johnson, K. Kendall, A. D. Roberts, *Proc. R. Soc. London. A. Math. Phys. Sci.* **1971**, *324*, 301.

[45] M. Ciavarella, *J. Tribol.* **2017**, *139*, 139.

[46] Y. H. Ting, C. C. Liu, S. M. Park, H. Jiang, P. F. Nealey, A. E. Wendt, *Polymers* **2010**, *2*, 649.

SUPPORTING INFORMATION